

MICROSCOPIC DYNAMICS OF HARD ELLIPSOIDS IN THEIR LIQUID AND GLASSY PHASE

A. Latz ¹, M. Letz ², R. Schilling and Th. Theenhaus ^a

^aInstitut für Physik, Johannes Gutenberg Universität, Mainz D-55099 Mainz, Staudinger Weg 7, Germany

¹ Institut für Physik, Reichenhainer Strasse 70, TU-Chemnitz, D-09107 Chemnitz, Germany

² Schott Glas, Research and Development, Hattenbergstr. 10, D-55014 Mainz, Germany

To investigate the influence of orientational degrees of freedom onto the dynamics of molecular systems in its supercooled and glassy regime we have solved numerically the mode-coupling equations for hard ellipsoids of revolution. For a wide range of volume fractions ϕ and aspect ratios x_0 we find an orientational peak in the center of mass spectra $\chi''_{000}(q, \omega)$ and $\phi''_{000}(q, \omega)$ about one decade below a high frequency peak. This orientational peak is the counterpart of a peak appearing in the quadrupolar spectra $\chi''_{22m}(q, \omega)$ and $\phi''_{22m}(q, \omega)$. The latter peak is almost insensitive on ϕ for x_0 close to one, i.e. for weak steric hindrance, and broadens strongly with increasing x_0 . Deep in the glass we find an additional peak between the orientational and the high frequency peak. We have evidence that this intermediate peak is the result of a coupling between modes with $l = 0$ and $l = 2$, due to the nondiagonality of the static correlators.

1. INTRODUCTION

Although experimental data on plastic crystals [1–3] have demonstrated that orientational degrees of freedom by themselves show glasslike dynamics and even can undergo a glass transition their role for the dynamics and the glass formation of supercooled liquids has not been studied in great detail. With the extension of mode-coupling theory (MCT) from simple liquids [4–7] to molecular systems [8–11] there is a *microscopic* theory which allows to investigate the role of the rotational degrees of freedom and their coupling to the translational ones. It is desirable to choose systems for which this coupling can be

varied systematically. From this point of view hard ellipsoids of revolution represent an interesting model system. Keeping their minor axis b fixed, a change of the aspect ratio $x_0 = a/b$, where a is the major axis, will change the steric hindrance between the ellipsoids. This again will result in a change of the translational-rotational coupling. Applying MCT to hard ellipsoids it was shown that for x_0 about two or larger the ellipsoids freeze into a glass at a critical volume fraction $\phi_c(x_0)$ due to the appearance of a medium range orientational order which originates from a precursor of a nematic order [12]. Recently we have shown that this precursor of nematic order also has an influence onto the dynamical features in the microscopic time and frequency regime [13]. From both, the solution of the corresponding MCT-equations and from a MD-simulation a peak in the compressibility spectrum has been found at ω_{op} about one decade below a high-frequency peak (hf-peak). The additional peak clearly has an orientational origin since ω_{op} scales with $I^{-1/2}$, I being the moment of inertia with respect to the minor axis. Therefore we called it an orientational peak (*op*). These calculations were restricted to a single aspect ratio, $x_0 = 1.8$, and one volume fraction, only. It is the motivation of the present contribution to study the microscopic dynamics and in particular the *op* as a function of x_0 and $\phi = \frac{\pi}{6}\varrho_0 x_0$ where ϱ_0 is the number density. In this respect we would also like to mention that studying the *athermal* system of hard ellipsoids can also be instructive for real molecular liquids composed of linear molecules like e. g. diatomic molecules. Indeed, it has been demonstrated that the static correlators $S_{lm,l'm'}(\vec{q})$ and the non-ergodicity parameters $f_{lm,l'm'}(\vec{q})$ for diatomic molecules with Lennard-Jones interactions obtained from a MD-simulation [14] can be well reproduced by a system of hard ellipsoids with $x_0 = 1.5$ [15]. Note that this aspect ratio was not the result of fitting procedure, but could be determined from the Lennard-Jones parameters.

Besides hard ellipsoids MCT has already been applied to study the dynamics of a dumbbell-molecule in an isotropic liquid of hard spheres [16], [17] and of a liquid of dipolar hard spheres [18]. Like for hard ellipsoids, the change of the elongation ζ of the dumbbell allows to vary the steric hindrance with the hard sphere environment. This effect has been investigated quantitatively for the orientational correlators $C_l(t) = \langle P_l(\vec{e}(t) \cdot \vec{e}(0)) \rangle$ where P_l are the Legendre Polynomials and $\vec{e}(t)$ is the unit vector pointing along the symmetry axis of the dumbbell at time t . It has been found that weak and strong steric hindrance can lead to quite different relaxational behavior. For instance, in case of sufficiently small elongations the α -relaxation scaling law is strongly disturbed. The correlator with odd- l and even- l behave different. It is interesting that this finding agrees with that found from a MD-simulation of a diatomic Lennard-Jones liquid. [19].

For dipolar hard spheres it is the dipolar interaction which is responsible for a translational-rotational-coupling. This type of coupling is different to that generated by steric hindrance. Nevertheless, we have also found in the compressibility spectrum an *op* about a decade below a hf-peak [18]. This may suggest that an *op* can be a rather general feature of a molecular liquid. This motivates to study for hard ellipsoids the microscopic dynamics as a function of the aspect ratio and volume fraction.

The organization of our paper is as follows. In the next section we will introduce the basic quantities and their equations of motion. The results from a numerical solution of these equations will be presented and discussed in section III and in section IV we will summarize and will give some conclusions.

2. Equations of motion: Hard ellipsoids

We consider a system of N hard ellipsoids of revolution with mass M and moment of inertia $I = M(1 + x_0^2)/20$ with respect to the minor axis. $x_0 = a/b$ is the aspect ratio, i.e. the ratio of the major and minor axis. The length and time unit is chosen such that $b = 1$ and $M = 1$. The microscopic configurations are given by the center of mass position \vec{x}_n and the set of Euler angles $\Omega_n = (\varphi_n, \vartheta_n, \chi_n)$, $n = 1, 2, \dots, N$. Because of the rotational invariance around the symmetry axis of the ellipsoids of revolution the third Euler angle χ_n is not involved in the steric hindrance. Consequently this degree of freedom will not be taken into account. Then, the basic quantities for the study of the molecular dynamics are the *tensorial* density correlators

$$S_{lm,l'm'}(\vec{q}, t) = \frac{1}{N} \langle \rho_{lm}^*(\vec{q}, t) \rho_{l'm'}(\vec{q}, 0) \rangle \quad (1)$$

where $\rho_{lm}(\vec{q}, t)$ is the microscopic tensorial density determined by $\{\vec{x}_n(t)\}$ and $\{\varphi_n(t), \vartheta_n(t)\}$. $l = 0, 1, 2, \dots$ and $-l \leq m \leq l$ specify the rotational part of the density modes. For completeness we mention that the dynamics of molecular liquids can also be described by a site-site formalism [9]. However, hard ellipsoids are not made up for a finite number of sites. Hence one has to approximate a hard ellipsoid by, e. g. a two-site dumbbell where each site is the center of a sphere as it was used in refs. [16], [17].

The correlation matrix $\mathbf{S}(\vec{q}, t) = (S_{lm,l'm'}(\vec{q}, t))$ simplifies as follows. First of all we can choose the q -frame, i.e. it is $\vec{q} = (0, 0, q)$, $q = |\vec{q}|$. This makes $\mathbf{S}(\vec{q}, t)$ diagonal in m [10]:

$$S_{lm,l'm'}(\vec{q}, t) = S_{l'm}(q, t) \delta_{mm'} \quad (2)$$

In addition one can prove [10] that $S_{ll'm}(q, t)$ are real and that

$$S_{ll'-m}(q, t) = S_{ll'm}(q, t). \quad (3)$$

Second the head-tail symmetry of the ellipsoids implies that the collective correlators $S_{lm,l'm'}(\vec{q}, t)$ vanish for l and/or l' odd. For its self part $S_{lm,l'm'}^{(s)}(\vec{q}, t)$, which will not be considered here, this is only true for $l + l'$ odd.

How to derive equations of motion for $\mathbf{S}(\vec{q}, t)$ has been described in great detail [10]. Here we repeat just the result:

$$\dot{\mathbf{S}}(\vec{q}, t) + i \sum_{\alpha=T,R} \mathbf{q}^\alpha \mathbf{S}^\alpha(\vec{q}, t) = 0 \quad (4a)$$

$$\begin{aligned} & \dot{\mathbf{S}}^\alpha(\vec{q}, t) + i \mathbf{q}^\alpha \mathbf{J}^\alpha(\vec{q}) \mathbf{S}^{-1}(\vec{q}) \mathbf{S}(\vec{q}, t) \\ & + \mathbf{J}^\alpha(\vec{q}) \int_0^t dt' \sum_{\alpha'=T,R} \mathbf{m}^{\alpha\alpha'}(\vec{q}, t-t') \mathbf{S}^{\alpha'}(\vec{q}, t') = 0 \end{aligned} \quad (4b)$$

with the initial conditions:

$$\begin{aligned} \mathbf{S}(\vec{q}, 0) &\equiv \mathbf{S}(\vec{q}), & \mathbf{S}^\alpha(\vec{q}, 0) &\equiv 0, \\ \dot{\mathbf{S}}(\vec{q}, 0) &\equiv 0, & \dot{\mathbf{S}}^\alpha(\vec{q}, 0) &\equiv -i \mathbf{J}^\alpha(\vec{q}) \mathbf{q}^\alpha \end{aligned} \quad (5)$$

and

$$(\mathbf{q}^\alpha)_{lm,l'm'} = \delta_{ll'} \delta_{mm'} \begin{cases} q & \alpha = T \\ \sqrt{l(l+1)} & \alpha = R \end{cases} \quad (6)$$

$$(\mathbf{J}^\alpha(\vec{q}))_{lm,l'm'} = (k_B T / I_\alpha) \delta_{ll'} \delta_{mm'} \quad (7)$$

where $I_T = M$ and $I_R = I$. $\mathbf{S}(\vec{q})$ and $\mathbf{J}^\alpha(\vec{q})$ are the static density and current density correlators, respectively. The form of this set of equations is different but equivalent to that derived in ref. [10]. The main difference is the occurrence of the density - current density correlators $\mathbf{S}^\alpha(\vec{q}, t)$ in Eqs. (4). It has been demonstrated that the set of equations (4) is appropriate for a numerical solution [18]. Eqs. (4) become closed by the MCT-approximation for the memory kernels $m_{lm,l'm'}^{\alpha\alpha'}(\vec{q}, t)$. With the shorthand notation $\lambda = lm$ it is [10]

$$\begin{aligned}
m_{\lambda\lambda'}^{\alpha\alpha'}(\vec{q}, t) &= \frac{1}{2N} \sum_{\vec{q}_1 \vec{q}_2} \sum_{\substack{\lambda_1 \lambda'_1 \\ \lambda_2 \lambda'_2}} \left(\sum_{\lambda''} [u^\alpha(\vec{q}\lambda|\vec{q}_1\lambda''; \vec{q}_2\lambda_2) c_{\lambda''\lambda_1}(\vec{q}_1) + (1 \leftrightarrow 2)] \right) \cdot \\
&\cdot \left(\sum_{\lambda'''} [u^{\alpha'}(\vec{q}\lambda'|\vec{q}_1\lambda'''; \vec{q}_2\lambda'_2) c_{\lambda'''\lambda'_1}(\vec{q}_1) + (1 \leftrightarrow 2)] \right)^* S_{\lambda_1\lambda'_1}(\vec{q}_1, t) S_{\lambda_2\lambda'_2}(\vec{q}_2, t) \quad (8)
\end{aligned}$$

where $u^T(\vec{q}\lambda|\vec{q}_1\lambda_1; \vec{q}_2\lambda_2)$ and $u^R(\vec{q}\lambda|\vec{q}_1\lambda_1; \vec{q}_2\lambda_2)$ are proportional to the Clebsh-Gordon coefficients $C(l_1 l_2 l; 000)$ and $C(l_1 l_2 l; 101)$, respectively. They vanish for $l+l_1+l_2$ odd, and their explicit form is given in [10]. The important input into (8) is the direct correlation matrix $\mathbf{c}(\vec{q}) = (c_{\lambda\lambda'}(\vec{q}))$ which is related to $\mathbf{S}(\vec{q})$ by the Ornstein-Zernike equation for linear molecules.

$$\mathbf{c}(\vec{q}) = (4\pi/\rho_0)[\mathbf{1} - \mathbf{S}^{-1}(\vec{q})] \quad , \quad (9)$$

where $\rho_0 = N/V$ is the number density.

Since we want to investigate the dependence of $\mathbf{S}(\vec{q}, t)$ on the aspect ratio it is important to check whether the Eqs. (4) and Eq.(8) reduce for $x_0 = 1$ to the corresponding equations of motion for hard spheres. Due to the complete isotropy of hard spheres it is:

$$c_{\lambda\lambda'}(\vec{q}) = \begin{cases} 4\pi c(\vec{q}), & (\lambda, \lambda') = (00, 00) \\ \equiv 0, & (\lambda, \lambda') \neq (00, 00) \end{cases} \quad (10)$$

where $c(\vec{q})$ is the direct correlation function for hard spheres. Substituting Eq.(10) into Eq. (8) strongly reduces the number of mode-coupling terms. First of all one obtains:

$$m_{\lambda\lambda'}^{\alpha\alpha'}(\vec{q}, t) \equiv 0, \quad (\alpha, \alpha') \neq (T, T) \quad (11)$$

Using $u^\alpha(\dots)$ from ref. [10] we get for the nonzero elements:

$$\begin{aligned}
m_{\lambda\lambda'}^{TT}(\vec{q}, t) &= \rho_0^2 \frac{1}{2N} \sum_{\vec{q}_1, \vec{q}_2} \left\{ \left(\frac{1}{q} \vec{q} \cdot \vec{q}_1 c(\vec{q}_1) \right)^2 S(\vec{q}_1, t) S_{\lambda\lambda'}(\vec{q}_2, t) + \right. \\
&+ \left(\frac{1}{q} \vec{q} \cdot \vec{q}_2 c(\vec{q}_2) \right)^2 S_{\lambda\lambda'}(\vec{q}_1, t) S(\vec{q}_2, t) + \\
&+ \left. \frac{1}{q^2} (\vec{q} \cdot \vec{q}_1)(\vec{q} \cdot \vec{q}_2) c(\vec{q}_1) c(\vec{q}_2) [S_{00,\lambda'}(\vec{q}_1, t) S_{\lambda,00}(\vec{q}_2, t) + (1 \leftrightarrow 2)] \right\} \quad (12)
\end{aligned}$$

where we used $S(\vec{q}, t) \equiv S_{00,00}(\vec{q}, t)$, the density correlator for hard spheres. Note that $m_{00,00}^{TT}(\vec{q}, t)$ coincides with the memory kernel for simple liquids in general and for hard spheres in particular. But $m_{\lambda\lambda'}^{TT}(\vec{q}, t)$ seems to be nondiagonal in λ . Such a nondiagonality would generate an *unphysical* influence (at least for hard spheres with smooth surfaces) of $S_{\lambda\lambda}(\vec{q}, t)$ with $\lambda \neq (0, 0)$ onto $S(\vec{q}, t)$. However, using the initial conditions Eq. (5) and

$$S_{\lambda\lambda'}(\vec{q}) = 0 \quad , \quad \lambda \neq \lambda' \quad (13)$$

which immediately follows from Eq. (9) and Eq. (10) one can prove that Eq. (4) and Eq. (8) yield:

$$\frac{d^\nu}{dt^\nu} S_{\lambda\lambda'}(\vec{q}, t)|_{t=0} = 0 \quad , \quad \lambda \neq \lambda' \quad (14)$$

for *all* ν . Although Eqs. (4) and (8) are nonlinear we therefore expect that Eq. (14) implies

$$S_{\lambda\lambda'}(\vec{q}, t) \equiv 0 \quad , \quad \lambda \neq \lambda' \quad , \quad (15)$$

as for linear equations. In that case $m_{\lambda\lambda'}^{\alpha\alpha'}(\vec{q}, t)$ given by Eq. (12) becomes diagonal in λ , i.e. the MCT-equations for the remaining correlators $S_{\lambda\lambda}(\vec{q}, t)$, $l \geq 0$, decouple with respect to λ . Therefore $S(\vec{q}, t)$ is not influenced by $S_{\lambda\lambda}(\vec{q}, t)$ with $\lambda \neq (0, 0)$ and it obeys the MCT-equation for hard spheres. Because $m_{\lambda\lambda}(\vec{q}, t)$ for $\lambda \neq (0, 0)$ contains bilinear terms $S(\vec{q}_1, t)S_{\lambda\lambda}(\vec{q}_2, t)$ the hard sphere correlator $S(\vec{q}, t)$ has an influence on the orientational correlators $S_{\lambda\lambda}(\vec{q}, t)$, which is unphysical, as well. The reason for this lies in our assumption that the density modes $\rho_\lambda(\vec{q})$ are slow variables for *all* λ , which only will be justified for $x_0 \neq 1$. Neglecting $\mathbf{m}(\vec{q}, t)$, Eqs. (4) reduce to a linear equation for the (normalized) correlators $\Phi(\vec{q}, t) = \mathbf{S}^{-1/2}(\vec{q})\mathbf{S}(\vec{q}, t)\mathbf{S}^{-1/2}(\vec{q})$ [18]:

$$\ddot{\Phi}(\vec{q}, t) + \mathbf{\Omega}^2(\vec{q})\Phi(\vec{q}, t) = 0 \quad (16)$$

with the hermitean frequency matrix squared:

$$\begin{aligned} (\mathbf{\Omega}^2(\vec{q}))_{lm, l'm'} = \\ = \sum_{l''m''} (\mathbf{S}^{-1/2}(\vec{q}))_{lm, l''m''} \left[\frac{k_B T}{M} q^2 + \frac{k_B T}{I} l''(l'' + 1) \right] (\mathbf{S}^{-1/2}(\vec{q}))_{l''m'', l'm'} \end{aligned} \quad (17)$$

These microscopic frequencies will play an essential role for our study of the microscopic dynamics. Since the static correlators $S_{lm,l'm'}(\vec{q})$ for hard ellipsoids are nondiagonal there will be a coupling between the various modes already on the linear level of Eq. (16). This type of coupling has been absent for dipolar hard spheres due to the use of Wertheim's solution for $c_{\lambda\lambda'}(\vec{q})$ for which the direct correlation functions are diagonal in l and l' [18]. Therefore in contrast to our results for dipolar hard spheres we may expect additional features for hard ellipsoids. The microscopic frequencies will become "renormalized" close to the glass transition and particularly deep in the glass. In ref. [18] it has been shown that the microscopic frequencies in the glass follow from:

$$(\widehat{\Omega}^2(\vec{q}))^{\alpha\alpha'} = (\mathbf{J}^\alpha(\vec{q}))^{1/2} [\mathbf{q}^\alpha \mathbf{S}^{-1}(\vec{q}) \mathbf{q}^{\alpha'} + \mathbf{C}^{\alpha\alpha'}(\vec{q})] (\mathbf{J}^{\alpha'}(\vec{q}))^{1/2} \quad (18)$$

with $C_{\lambda\lambda'}^{\alpha\alpha'}(\vec{q}) = \lim_{t \rightarrow \infty} m_{\lambda\lambda'}^{\alpha\alpha'}(\vec{q}, t)$.

3. Results

To solve Eqs. (4) and Eqs. (8) numerically one has to cut-off q and l . Since the numerical effort is considerable for hard ellipsoids we have chosen $l \leq l_{co} = 2$ and 30 q -values which were distributed non-equidistantly between $q_{min} \cong 0.51$ and $q_{co} = 40$.

More details about the numerical procedure can be found in ref. [18]. Furthermore we have restricted ourselves to $x_0 > 1$. Although no strict symmetry exists between $x_0 > 1$ and $x_0 < 1$ one may expect similar behavior for $x_0 < 1$. It would be interesting to check this point. The direct correlation functions needed as an input for the memory kernels were calculated from Percus-Yevick theory [21]. The temperature enters into $\mathbf{J}^\alpha(\vec{q})$, only (cf. Eq. (7)). We choose $k_B T$ such that the thermal velocity $(k_B T/M)^{1/2}$ equals one. This choice also sets the scale for the microscopic frequencies $\Omega_{lm,l'm'}^{\alpha\alpha'}(\vec{q})$ and $\widehat{\Omega}_{lm,l'm'}(\vec{q})$. All results will be given for the q -frame.

Before we come to the dynamical results we present in figure 1 the phase diagram. The liquid phase is below the solid line and bounded by the thick part of the dashed line. The remaining part corresponds to the glassy phase. This diagram contains two glass transition lines which cross at $(\phi, x_0) \cong (0.498, 2.42)$. This crossing relates to a change of the mechanism for the glass transition. For $1 \leq x_0 < 2.42$ it is the cage effect which mainly leads to a freezing into a glass whereas for $x_0 > 2.42$ a precursor of a nematic order becomes responsible for the glass transition [12]. Note, that this change at $x_0 \cong 2.42$ does not happen suddenly but it is a crossover phenomenon. Therefore the numerical value $x_0 \cong 2.37$ should not be over-interpreted.

The correlators $S_{ll'm}(q, t)$ for $l \leq l_{co} = 2$ and $q \leq q_{co} \cong 40$ were calculated from Eqs. (4) and (8) for the points shown in figure 1. From these results we have determined the correlation spectra $\phi''_{ll'm}(q, \omega)$ and the susceptibility $\chi''_{ll'm}(q, \omega) = \omega \phi''_{ll'm}(q, \omega)$. Figure 2 presents the compressibility spectrum for $q \cong 4.2$ and pairs of (ϕ, x_0) on the liquid side, but close to the glass transition line (full symbols in figure 1). Here we include $x_0 = 1.8$ for which the static correlators were obtained from a MD-simulation [13]. We have chosen double-logarithmic scales on which the characteristic features become more prominent. For hard spheres, i.e. $x_0 = 1$, only one peak, which we called the high frequency peak (hf-peak), exists at ω_{hf} for $\omega \geq 10^{-1}$. Now, making x_0 larger than one, we observe an additional peak at ω_{op} about one decade below the hf-peak. This peak is what we called the orientational peak (*op*) in the first section. It already appears for $x_0 = 1.1$, the smallest value we have chosen besides $x_0 = 1$. With increasing aspect ratio, up to our maximum value $x_0 = 2$, the position of the *op* almost does not change whereas ω_{hf} first increases and then decreases. The most striking features are (i) the *op* becomes broader and (ii) the ratio of the height of the *op* and the hf-peak increases with increasing x_0 . This behavior can be understood as follows. Increasing x_0 enhances the steric hindrance which leads to a stronger translational-rotational-coupling. Therefore the orientational motion which is an almost free rotation with a single frequency for x_0 close to one couples stronger and stronger to the translational motion which enters into the compressibility. This leads to a more hindered rotational motion involving a broader band of rotational frequencies such that the *op* becomes broader and it leads to an enhancement of the orientational contribution at ω_{op} relative to the translational one at ω_{hf} . Since ω_{hf} does not change with I [13] it must be related to the translational motion. The fact that a distinct "fingerprint" of the orientational dynamics can be observed in the compressibility spectrum already for $x_0 = 1.1$ might be surprising. But figure 3 supplies an explanation. There we show $\chi''_{ll'm}(4.2, \omega)$ and $\phi''_{ll'm}(4.2, \omega)$ on linear scales, for the volume fractions marked in figure 1 for $x_0 = 1.1$. Because these quantities for $(ll'm) = (200), (221)$ and (222) strongly resemble that for $(ll'm) = (220)$ we only show data for (000) and (220) . $\chi''_{220}(4.2, \omega)$ and $\phi''_{220}(4.2, \omega)$ exhibit one rather sharp peak at $\omega'_{op} \approx 8$. For $x_0 = 1$ it follows from Eq. (9) with Eq. (10) that $S_{lm,l'm'}(\vec{q}) = \delta_{ll'}\delta_{mm'}$ for $l > 0$. Using this, $q = 0$ and $I = 1/10$ (for $x_0 = 1$) we get from Eq. (17) the frequency $\Omega_2^{\text{free}} = (10 \cdot 2 \cdot 3)^{1/2} \cong 7.75$ for a free rotation of a sphere with $l = l' = 2$. Therefore it is obvious that the peak in χ''_{220} and ϕ''_{220} at $\omega'_{op} \approx 8$ comes from an almost free rotation. If the rotation is *completely* free then $\chi''_{220}(q, \omega)$ and $\phi''_{220}(q, \omega)$ are proportional to $\delta(\omega - \Omega_2^{\text{free}})$. Although the coupling of the rotational motion into χ''_{000} is very small for $|1 - x_0| \ll 1$ it is the almost δ -like

behavior of $\chi''_{220}(q, \omega)$ and $\phi''_{220}(q, \omega)$ which can contribute significantly to $\chi''_{000}(q, \omega)$ and $\phi''_{000}(q, \omega)$. This contribution is more apparent for χ''_{000} than for ϕ''_{000} , as can be seen from figure 3. Whereas the *op* at $\omega_{op} \approx \Omega_2^{\text{free}}$ occurs in χ''_{000} for all studied volume fractions it only becomes present in ϕ''_{000} closer to the glass transition. The fact that $\omega_{op} \approx \omega'_{op}$ supports the rotational origin of the *op*. Two more features follow. First, the spectra for $(ll'm) = (000)$ depend sensitively on ϕ whereas those for $(ll'm) = (220)$ almost do not change, and second ω_{op} is practically constant in contrast to the position ω_{hf} of the hf-peak which moves towards higher frequencies with increasing ϕ . The latter observation implies that with increasing ϕ the glass becomes more stiff with respect to the translational than for the rotational dynamics, provided x_0 is close to one.

Now let us consider the results for the largest value for x_0 we have studied. Figure 4 presents the spectra (again on linear scales) for $x_0 = 2$ and the volume fractions indicated in figure 1. The glass transition occurs at $\phi_c(x_0 = 2) \cong 0.545$. Comparison of figure 4 with figure 3 shows that all the spectra have become more structured and broader due to the increase of x_0 . The rather narrow peak in $\chi''_{220}(4.2, \omega)$ and $\phi''_{220}(4.2, \omega)$ at $\omega'_{op} \approx 8$ for $x_0 = 1.1$ has almost disappeared. It occurs as a shoulder in χ''_{220} and as a peak in ϕ''_{220} deeper in the glass. Its shape and intensity depends on ϕ . A well pronounced peak also occurs in χ''_{220} and ϕ''_{220} at ω_{int} between $\omega \approx 15$ and $\omega \approx 25$, depending on ϕ . This peak is present in the liquid ($\phi \leq 0.54$) and the glass ($\phi \geq 0.55$).

These two peaks have their counterparts in χ''_{000} and ϕ''_{000} at $\omega_{op} \approx \omega'_{op}$ and $\omega_{int} \approx \omega'_{int}$, although the peak in χ''_{000} at $\omega \approx \omega_{int}$ becomes more pronounced deeper in the glass, and has a shoulder-like behavior for ϕ''_{000} , only. Besides these two peaks a hf-peak exists above $\omega \approx 25$, for all volume fractions. We have checked the dependence of these peak positions on the moment of inertia I and have found that only $\omega_{op} \approx \omega'_{op}$ shifts with I . Therefore the peak at $\omega_{op} \approx \omega'_{op}$, which is much less pronounced than for $x_0 = 1.1$ is the orientational peak. The origin of the intermediate peak will be elucidated below.

It is also interesting to study the q -dependence of the spectra. This has been done for an intermediate aspect ratio $x_0 = 1.5$ and $\phi = 0.64$, i.e. deep in the glass (cf. figure 1). The result is depicted in figure 5 for $\phi''_{l0}(q, \omega)$ and $l = 0, 2$. The q -dependence of $\chi''_{l0}(q, \omega)$ is quite similar. Even more pronounced than for $x_0 = 2$ we observe two peaks in ϕ''_{220} at $\omega'_{op} \approx 10 - 20$ and at $\omega'_{int} \approx 35$. Again, these two peaks have their counterpart in $\phi''_{000}(q, \omega)$ at ω_{op} and ω_{int} . In addition there is a hf-peak at ω_{hf} . The dispersion of these peak positions depends on l . ω_{op} is practically q -independent whereas ω'_{op} exhibits some q -dependence, and the position of the intermediate and the hf-peak shows dispersion for $l = 0$ and $l = 2$.

To understand the existence and the q -dependence of these peaks at least qualitatively we have calculated for $x_0 = 1.5$, $\phi = 0.64$ and $l \leq l_{co} = 2$ the eigenfrequencies $\Omega_3^\pm(q)$ of the 2×2 matrix $(\Omega_{l_0, \nu_0}(q))$, $\Omega_1(q) \equiv \Omega_{21, 21}(q)$, $\Omega_2(q) \equiv \Omega_{22, 22}(q)$ and the "renormalized" frequencies $\hat{\Omega}_\nu(q)$, $\nu = 1, 2$ and 3 which are the eigenfrequencies of the 3×3 matrix $(\hat{\Omega}_{l_0, \nu_0}^{\alpha\alpha'}(q))$ (cf. [18]). Since $\hat{\Omega}_{l_0, \nu_0}^{RR}(q) = 0$ for l and/or l' equal to zero, $(\hat{\Omega}_{l_0, \nu_0}^{\alpha\alpha'}(q))$ is indeed a 3×3 matrix for $l, l' \leq 2$. The results for $\Omega_\nu(q)$ and $\hat{\Omega}_\nu(q)$ are given in figure 6a and 6b, respectively. Figure 6b also contains $\omega_{op}(q)$, $\omega_{int}(q)$ and $\omega_{hf}(q)$ determined from $\phi''_{000}(q, \omega)$ for $x_0 = 1.5$ and $\phi = 0.64$, i.e. deep in the glass. Since $\Omega_1(q)$ cannot be distinguished from $\Omega_2(q)$ there are practically three branches in figure 6a. Because $\Omega_3^+(q) \rightarrow 0$ for $q \rightarrow 0$ it is the longitudinal acoustic branch, whereas the others are optic-like. These optic-like behavior also appears for the "renormalized" frequencies $\hat{\Omega}_1(q)$ and $\hat{\Omega}_2(q)$ which seem to reproduce at least qualitatively the results for $\omega_{op}(q)$ and $\omega_{int}(q)$. The same holds for $\omega_{hf}(q)$ which is in phase with $\hat{\Omega}_3(q)$ where $\hat{\Omega}_3(q)$ is the "renormalized" bare frequency $\Omega_3^+(q)$. Unfortunately, our results for $\hat{\Omega}_\nu(q)$ become less accurate for small q . For an explanation see ref. [18]. Therefore we cannot definitely determine the dispersion for $q \rightarrow 0$. The intermediate peak only appears deep in the glass. In that case the nondiagonal static correlator $S_{200}(q)$ becomes large. Therefore we believe that the origin of that peak comes from the additional coupling between the modes with $l = 0$ and $l = 2$ which already exists on the linear level (see discussion at the end of section 2).

4. Summary and conclusions

We have calculated the dynamics of a system of hard ellipsoids as a function of the volume fraction ϕ and the aspect ratio x_0 . In the spectra for the center of mass dynamics we have found an orientational peak at ω_{op} , roughly one decade below a high-frequency peak. Due to its shift with the moment of inertia and its appearance in the spectra of the "quadrupolar" motions (quantities with $\ell = 2$) its origin is mainly of orientational nature. This peak becomes broader and its intensity relative to the intensity of the hf-peak increases with increasing x_0 , i.e. with the increase of the steric hindrance. Its position is practically q -independent and it scales with $I^{-1/2}$. This implies that it originates mainly from localized modes with $q \approx 0$, as already found in refs. [13] and [18]. For the dipolar hard sphere system studied in ref. [18] it has also been speculated that this orientational peak could be one of several contributions to the *boson peak*. Since hard ellipsoids are an athermal system we can not draw such a conclusion here. However, the appearance of the *op* for all aspect ratios we have studied together with its existence for dipolar hard

spheres may give a hint that it may occur in many molecular liquids. That it is not an artefact of the approximate character of the used equations of motions has clearly been demonstrated by the MD-simulation [13].

It is also interesting for x_0 close to one that a variation of ϕ almost does not affect the spectra for $l = l' = 2$, in contrast to those for $l = l' = 0$. There is a significant influence of the rotational motion on χ''_{000} and ϕ''_{000} but much less feedback from the translational motion to χ''_{220} and ϕ''_{220} for weak steric hindrance.

Finally, deep in the glass we have found an intermediate peak between the *op* and hf-peak. This peak did not appear for dipolar hard spheres where the static correlators were taken diagonal in l and l' . Since this is not the case for the system of hard ellipsoids we believe that the intermediate peak turns up due to a coupling between modes with $l = 0$ and $l = 2$ mediated by the nondiagonal elements of $S_{ll'm}(q)$. The q -dependence of the orientational, intermediate and the hf-peak in the compressibility spectrum can be described by the "renormalized" eigenfrequencies, at least on a qualitative level.

Acknowledgement: We gratefully acknowledge financial support by the "Sonderforschungsbereich 262" (Deutsche Forschungsgemeinschaft) of the present research project and of those during the last ten years.

REFERENCES

1. M. A. Ramos, S. Viera, E. J. Bermejo, J. Dawidowski, H. E. Fischer, H. Schober, M. A. Gonzalez, C. K. Loong and D. L. Price, *Phys. Rev. Lett.* **78** (1997) 82.
2. H. E. Fischer, E. J. Bermejo, G. J. Cuello, M. T. Fernandez-Diaz, J. Davidowski, M. A. Gonzalez, H. Schober and H. Jimenez-Ruiz, *Phys. Rev. Lett.* **82** (1999) 1193.
3. F. Affouard and M. Descamps, *Phys. Rev. Lett.* **87** (2001) 035501.
4. W. Götze in, *Liquids, Freezing and the Glass transition*, (edited by J. P. Hansen, D. Levesque and J. Zinn-Justin, North-Holland, Amsterdam 1991).
5. W. Götze and L. Sjögren, *Rep. Prog. Phys.* **55** (1992) 241.
6. R. Schilling, *Disorder Effects on Relaxation Processes*, (edited by R. Richter and A. Blumen, Springer, Berlin 1994).
7. H. Z. Cummins, *J. Phys.: Condens. Matter*, **11** (1999) A95.
8. T. Franosch, M. Fuchs, W. Götze, M. R. Mayr and A. P. Singh, *Phys. Rev. E* **56** (1997) 5659.
9. S.-H. Chong and F. Hirata, *Phys. Rev. E* **58** (1998) 6188.
10. R. Schilling and T. Scheidsteger, *Phys. Rev. E* **56** (1997) 2932.
11. L. Fabbian, A. Latz, R. Schilling, F. Sciortino, P. Tartaglia, and C. Theis, *Phys. Rev. E* **60** (1999) 5768.
12. M. Letz, R. Schilling and A. Latz, *Phys. Rev. E* **62**, 5173 (2000).
13. Th. Theenhaus, M. Letz, A. Latz, R. Schilling and M. Allen, in preparation
14. S. Kämmerer, W. Kob and R. Schilling, *Phys. Rev. E* **58** (1998) 2141.
15. M. Letz and R. Schilling, *Phil. Mag. B* **79** (1999) 1815.
16. W. Götze, A. P. Singh and T. Voigtmann, *Phys. Rev. E* **61** (2000) 6934.
17. S.-H. Chong, W. Götze and A. P. Singh, *Phys. Rev. E* **63** (2000) 011206.
18. T. Theenhaus, R. Schilling, A. Latz and M. Letz, *Phys. Rev. E* in print; cond-mat 0105393.
19. S. Kämmerer, W. Kob and R. Schilling, *Phys. Rev. E* **56** (1997) 5450.
20. J. P. Hansen and I. R. McDonald, *Theory of Simple Liquids* (Academic Press, London, 2nd Edition, 1986).
21. M. Letz and A. Latz, *Phys. Rev. E* **60** (1999) 5865.

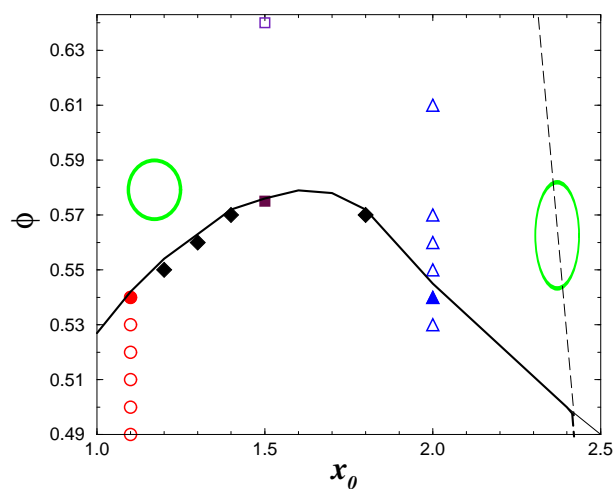


Figure 1. Glass transition phase diagram for hard ellipsoids: There are two glass transition lines (solid and dashed lines). See text for an explanation. The symbols show those points for which we have calculated the time-dependent correlators. To demonstrate the deviation from a hard sphere the cross section of an ellipsoid is shown for $x_0 = 1.1$ and $x_0 = 2.4$.

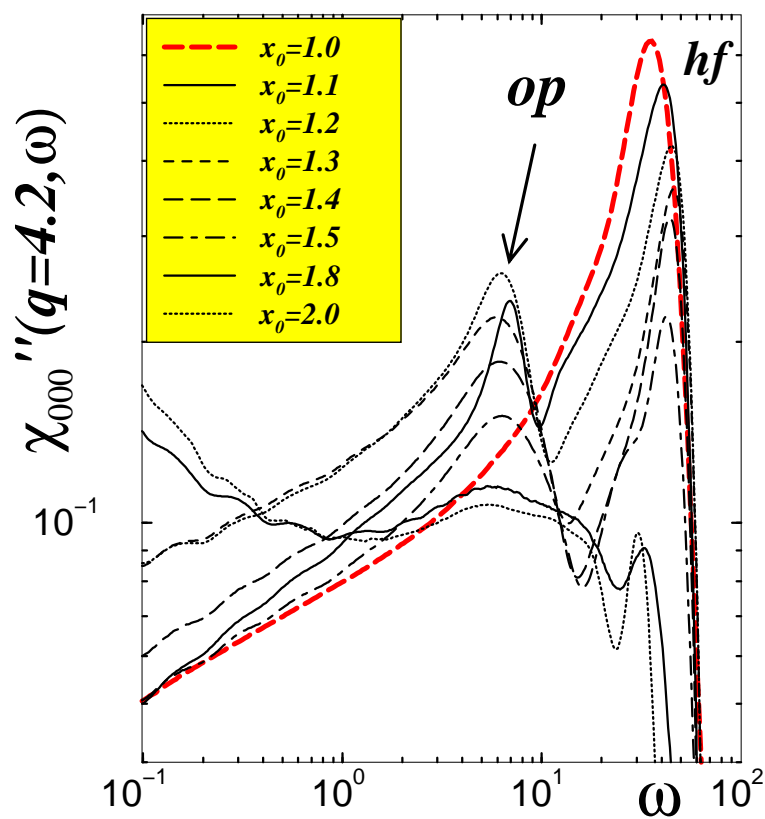


Figure 2. Compressibility $\chi''_{000}(4.2, \omega)$ for (ϕ, x_0) indicated by the full symbols in figure 1. The result for hard spheres ($x_0 = 1$) with $\phi = 0.5184$ is shown by the thick dashed line.

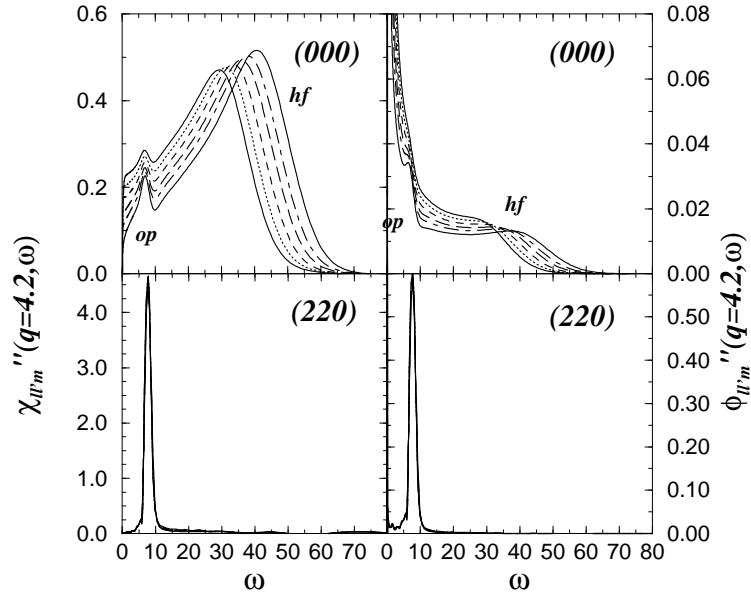


Figure 3. ω -dependence of $\chi''_{ll_0}(4.2, \omega)$ (left) and $\phi''_{ll_0}(4.2, \omega)$ (right) for $l = 0, 2$, $x_0 = 1.1$ and the ϕ -values marked in figure 1: $\phi = 0.49$ (solid) 0.50 (dotted) 0.51 (short dashed) 0.52 (long dashed) 0.53 (chain) 0.54 (solid)

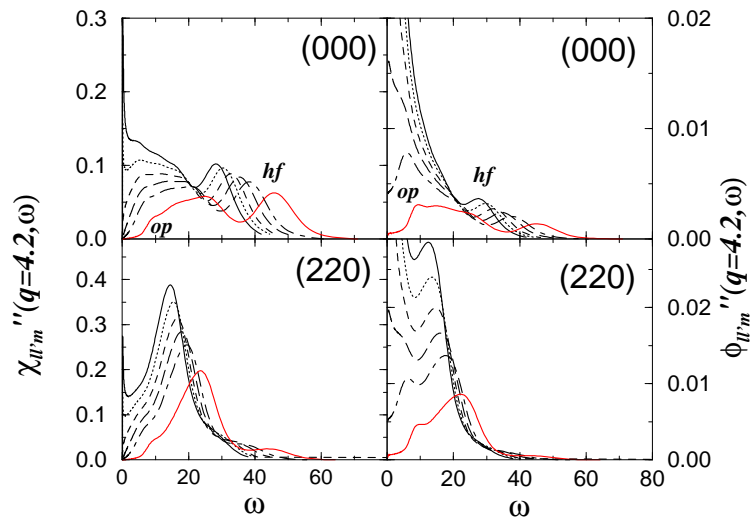


Figure 4. ω -dependence of $\chi''_{ll_0}(4.2, \omega)$ (left) and $\phi''_{ll_0}(4.2, \omega)$ (right) for $l = 0, 2$, $x_0 = 2$ and the ϕ -values marked in figure 1: $\phi = 0.53$ (solid) 0.54 (dotted) 0.55 (short dashed) 0.56 (long dashed) 0.57 (chain) 0.61 (solid)

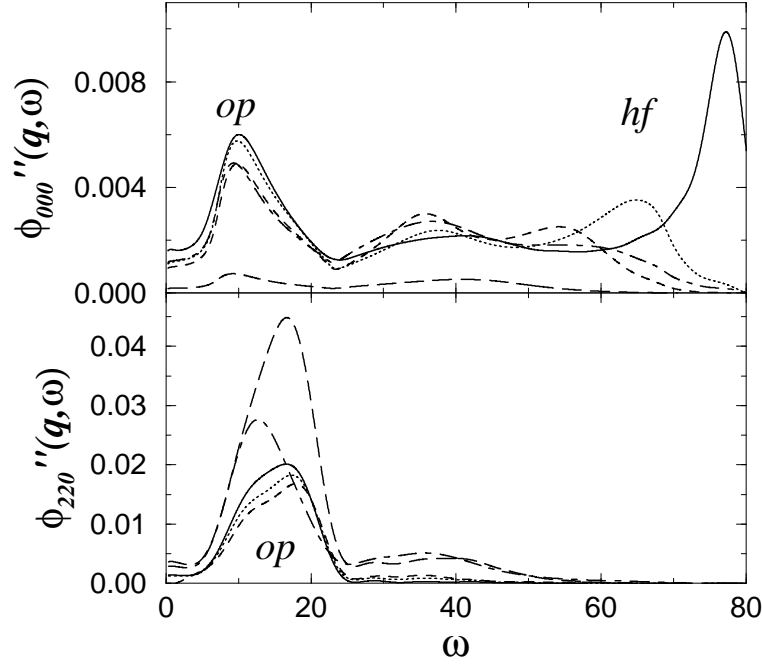


Figure 5. ω -dependence of $\phi''_{l0}(q, \omega)$ for $l = 0, 2$, $x_0 = 1.5$, $\phi = 0.64$ and $q = 3.1$ (solid line), 4.2 (dotted line), 4.7 (short dashed line), 6.5 (long dashed line) and 9.8 (chain line)

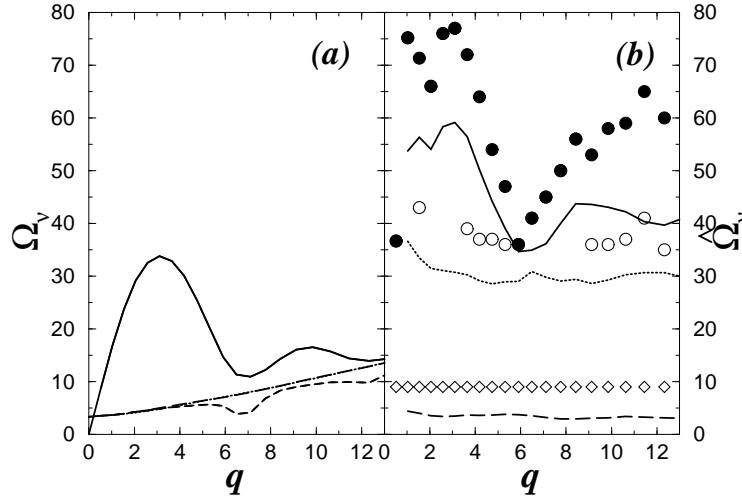


Figure 6. q -dependence of (a) Ω_3^+ (solid line), Ω_3^- (short dashed line), Ω_1 (long dashed line) and Ω_2 (dotted line) (see text). (b) $\hat{\Omega}_1$ (dashed line), $\hat{\Omega}_2$ (dotted line) and $\hat{\Omega}_3$ (solid line) (see text). The peak positions ω_{op} (diamonds), ω_{int} (open circles) and ω_{hf} (full circles) were deduced from $\phi''_{000}(q, \omega)$ for $x_0 = 1.5$ and $\phi = 0.64$.